



Czajka, A., Hill, C., Peach, J., Pegg, J. C., Grillo, I., Guittard, F., ... Eastoe, J. (2017). Trimethylsilyl hedgehogs - A novel class of super-efficient hydrocarbon surfactants. *Physical Chemistry Chemical Physics*, 19(35), 23869-23877. <https://doi.org/10.1039/c7cp02570j>

Peer reviewed version

License (if available):  
Unspecified

Link to published version (if available):  
[10.1039/c7cp02570j](https://doi.org/10.1039/c7cp02570j)

[Link to publication record in Explore Bristol Research](#)  
PDF-document

This is the author accepted manuscript (AAM). The final published version (version of record) is available online via Royal Society of Chemistry at <http://pubs.rsc.org/en/Content/ArticleLanding/2017/CP/C7CP02570J#!divAbstract>. Please refer to any applicable terms of use of the publisher.

## University of Bristol - Explore Bristol Research

### General rights

This document is made available in accordance with publisher policies. Please cite only the published version using the reference above. Full terms of use are available: <http://www.bristol.ac.uk/pure/about/ebr-terms>

Cite this: DOI: 10.1039/xxxxxxxxxx

# Trimethylsilyl Hedgehogs - A novel class of super-efficient hydrocarbon surfactants<sup>†</sup>

Adam Czajka,<sup>a</sup> Christopher Hill,<sup>a</sup> Jocelyn Peach,<sup>a</sup> Jonathan C. Pegg,<sup>a</sup> Isabelle Grillo,<sup>b</sup> Frédéric Guittard,<sup>c</sup> Sarah E. Rogers,<sup>d</sup> Masanobu Sagisaka,<sup>e</sup> and Julian Eastoe<sup>a\*</sup>

Received Date


Accepted Date


DOI: 10.1039/xxxxxxxxxx



www.rsc.org/journalname

Presented here are results for a novel class of hydrocarbon surfactants, termed *tetramethylsilyl hedgehogs* (TMS-hedgehogs), due to the presence of silicon in the tails. By comparing the surface properties of these hybrid hedgehogs to purely hydrocarbon equivalents, links between performance and structure are made. Namely, by controlling the molecular volume of the surfactant fragments, improvements can be made in surface coverage, generating lower surface energy monolayers. Small-angle neutron scattering (SANS) data has been collected showing these novel surfactants aggregate to form ellipsoidal micelles which grow with increasing concentration. This study highlights the sensitive relationship between surface tension and the surfactant chain, for design of new super-efficient surfactants close to the limit of the lowest surface tensions possible.

## 1 Introduction

Surfactants exhibit diverse behaviour  fascinating with useful properties owing to their amphiphilic character. In aqueous systems they will spontaneously adsorb to the interface, forming orientated monolayers which lower the surface tension  $\gamma$  (surface energy). Therefore, one of the most commonly measured properties of surfactants is their ability to reduce surface tension.<sup>1–5</sup> Many industrial processes require low surface energy to operate optimally and therefore, surfactants find uses in numerous applications including: agrochemicals, pharmaceuticals, cosmetics, detergents, petroleum, paints, coatings, adhesives and printing.<sup>6</sup> The most effective surfactants (i.e. showing the greatest reduction in  $\gamma$ ) are fluorocarbon (FC) surfactants, able to reduce  $\gamma$  for water from ca. 72 mNm<sup>-1</sup> to 15–25 mNm<sup>-1</sup> (25 °C). However, it has been identified that fluorinated compounds are environmentally hazardous pollutants which bioaccumulate, and hence, there is now a need to develop replacements for FC surfactants.<sup>7,8</sup> Generally, hydrocarbon (HC) surfactants are only able to reduce

the surface tension of water to  $\approx 30$  mNm<sup>-1</sup>.<sup>9</sup> How  highly branched hydrocarbon or "hedgehog" surfactants are a new class of low-surface energy surfactants with surface properties rivaling fluorosurfactants.<sup>10,11</sup>

The surface tension ( $\gamma$ ) generated by surfactants is intimately related to surface intermolecular interactions, which are strongly influenced by the chemical identity of the surfactant tails, amongst other characteristics.<sup>12,13</sup> Hence, the hydrophobic tails have a major effect controlling important physiochemical properties such as the critical micelle concentration (cmc), and limiting values at the cmc of area per molecule  $A_{\text{cmc}}$ , surface excess  $\Gamma_{\text{cmc}}$ , surface coverage  $\Phi_{\text{cmc}}$  (see equation 3 in §3.2) and surface tension  $\gamma_{\text{cmc}}$ . Because these properties are characteristic  any given surfactant, they are useful parameters to compare performance and identify structure-property relationships. By comparing the performance of three classes of surfactants (fluoro/silicone/hydrocarbon) in terms of  surface packing index  $\Phi_{\text{cmc}}$ , a general structure-property relationship of surfactants was identified: the limiting tension  $\gamma_{\text{cmc}}$  depends on the ability of surfactant hydrophobic tails to efficiently pack and form dense surface layers.<sup>14</sup> For super-efficient hydrocarbon surfactants, the tails should pack to mimic the density of a pure alkane and result in  $\Phi_{\text{cmc}}$  close to 1 (i.e. dense surface packing).

When present in water, the common linear hydrocarbon surfactant sodium dodecylsulfate (SDS) achieves a  $\gamma_{\text{cmc}} = 35$  mNm<sup>-1</sup>,<sup>15</sup> much higher than the corresponding liquid alkane, dodecane  $\gamma = 25.35$  mNm<sup>-1</sup> at 20 °C. This is because the water soluble headgroups present in surfactants sterically hinder the hydrophobic tails from efficiently packing to form dense surface coverages, as well as increasing the dispersion contribution  $\gamma^{\text{d}}$

<sup>a</sup> School of Chemistry, University of Bristol, Cantock's Close, Bristol, BS8 1TS. Tel: +44 0117 928 9180; E-mail: julian.esatoe@bristol.ac.uk

<sup>b</sup> Institut Laue-Langevin, 71 avenue des Martyrs - CS 20156 - 30842 Grenoble Cedex 9.

<sup>c</sup> University of Nice Sophia Antipolis, CNRS, LPMC, Group surfaces & interfaces, Parc Valrose, 06100 Nice, France.

<sup>d</sup> ISIS Neutron and Muon Source, Rutherford Appleton Laboratory, Didcot, OX11 0QX.

<sup>e</sup> Department of Frontier Materials Chemistry, Hirosaki University, 3 Bunkyo-cho, Hirosaki, Aomori 036-8561, Japan.

<sup>†</sup> Electronic Supplementary Information (ESI) available and includes: Full characterisation of all new compounds by <sup>1</sup>H, <sup>13</sup>C and EA. Example showing how cmcs were determined. Full details of all models used in fitting the scattering data. See DOI: 10.1039/b000000x/

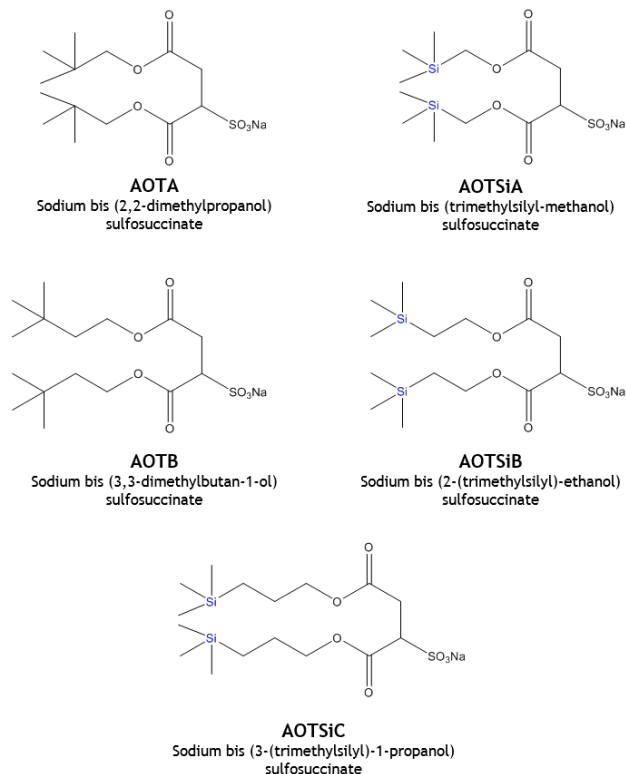


**Fig. 1** Molecular structures of the surfactants investigated in this article

to the total tension by introducing dipolar interactions. Therefore, to promote water solubility, which is essential for surfactant molecules, dipolar interactions are both essential and unavoidable. Highly branched HC surfactants, termed "hedgehog" surfactants due to their spiky brushlike structures, have achieved  $\gamma_{\text{cmc}} = 24.6 \text{ mN m}^{-1}$  (ref 10), much lower than the corresponding linear chain C18 hydrocarbon surfactant ( $\gamma_{\text{cmc}} = 33.2 \text{ mN m}^{-1}$ ) and indeed lower than certain dichain FC surfactants, e.g.  $26.8 \text{ mN m}^{-1}$  for DiHCF<sub>2</sub>. This remarkable reduction in surface tension is thought to be due to 1) a direct increase in the  $-\text{CH}_3$  to  $-\text{CH}_2-$  ratio per headgroup based on the following order of increasing surface energy  $\text{CF}_3 < \text{CF}_2 < \text{CH}_3 < \text{CH}_2$  (ref 13), and 2) chain branching drives  $A_{\text{cmc}}$  higher because of the increased bulkiness of the tails, which causes a decrease in the number of surfactant molecules per unit area and therefore, fewer tail-tail interactions between chains. Previously, a series of dichain hedgehog surfactants were developed with a design strategy to incorporate as many low surface energy groups ( $\text{CH}_3$ ) as possible in the hydrophobic tails (ref. 11). From this series, the most efficient surfactant, di-BC<sub>2</sub> achieves  $\gamma_{\text{cmc}} = 23.8 \text{ mN m}^{-1}$  (at  $35^\circ\text{C}$ ) with a  $\Phi_{\text{cmc}} = 0.95$  (i.e. a high surface coverage), highlighting that short branched HC surfactants can effectively lower the surface tension of water.

Here, a novel series of short branched HC surfactants are introduced, see Figure 1, generating surface tensions as low as  $\gamma_{\text{cmc}} = 22.8 \text{ mN m}^{-1}$  at  $25^\circ\text{C}$ . This has been achieved by incorporating silicon directly into the hydrocarbon chain to slightly increase the surfactant tail volume, making further improvements in packing efficiency. To discuss the effects of chain silylation and to iden-

tify how this helps to produce a low surface energy, hydrocarbon analogues have also been synthesised (AOTA has previously been referred to as AOT14,<sup>17</sup> and the hydrocarbon equivalent of AOTSiC could not be synthesised in sufficient quantities due to expensive starting materials). Surface properties are discussed and compared between the two series, as well as the aggregation structures formed in solution, studied using Small-Angle Neutron Scattering (SANS). Hence, these are not conventional, purely hydrocarbon hedgehog surfactants but trimethylsilyl hedgehogs, or TMS-hedgehogs for short, consisting of carbon and silicon. to be confused with silicone, or siloxane surfactants which are a distinctively different class. A characteristic of silicone surfactants is a highly flexible  $-\text{O}-\text{Si}-\text{O}-\text{Si}-$  backbone. However, the  $\text{Si}-\text{O}-\text{Si}$  linkage is susceptible to hydrolysis in the presence of moisture,<sup>18</sup> and the hydrolytic instability of silicone surfactants is an inherent weakness which reduces their performance. The TMS-hedgehogs introduced here have been designed to circumvent both the hydrolytic instability of silicone surfactants, and the environmentally hazardous nature of fluorosurfactants, whilst generating the lowest surface energies currently achieved by HC surfactants.

## 2 Experimental

### 2.1 Materials

The synthesis of dichain surfactants has been described before.<sup>19</sup> The materials used were 2,2-Dimethyl-1-propanol (Aldrich 99%), (Trimethylsilyl)methanol (Aldrich 98%), 3,3-Dimethyl-1-butanol (Aldrich 98%) 2-(Trimethylsilyl)ethanol (Aldrich 99%) and 3-(Trimethylsilyl)-1-propanol (Aldrich 97%), Dimethylaniline (Aldrich 99%), Fumaryl chloride (Aldrich 95%), Tetrahydrofuran (Aldrich 99%+ anhydrous), Hexane (Aldrich 98%), Ethyl acetate (Aldrich; 99.8%+ anhydrous), Hydrochloric acid (Aldrich 98%), Diethyl ether (VWR Chemicals; 95%), Methanol (Aldrich; 99.8%+ anhydrous), Anhydrous magnesium sulfate (VWR Chemicals 65/70%), Sodium hydrogen carbonate (Aldrich 98%), Sodium metabisulfite (Aldrich 98%), Sodium sulphite (Aldrich 98%) and Ethylenediaminetetraacetic acid tetrasodium salt hydrate (Aldrich 98%)

### 2.2 Surfactant synthesis

The same synthetic procedure was used for all surfactants shown in Figure 1, as an example, the synthesis of AOTA is outlined here. Neopentyl alcohol (8.055 g, 2.2 eq.) and dimethylaniline (10.069, 2.0 eq.) were dissolved in 150 mL dry tetrahydrofuran. The reaction vessel was flushed with  $\text{N}_2$  and then fumaryl chloride (6.355 g, 1.0 eq.) was added dropwise. As the fumaryl chloride was added the internal temperature rose to approximately  $65^\circ\text{C}$ . Once all the fumaryl chloride was added, the reaction mixture was refluxed and TLC plates developed periodically (4:1 hexane:ethyl acetate eluent) to check for residual fumaryl chloride. After approximately 4 hours the reaction was complete and THF was removed by rotary evaporation. The product was dissolved in diethyl ether and the ethereal solution was washed sequentially with 10 % hydrochloric acid ( $100 \text{ cm}^3$ ) and saturated aqueous sodium hydrogen carbonate solution ( $100 \text{ cm}^3$ ) until the aqueous

phase was clear. The washed ethereal solution was dried over anhydrous magnesium sulfate, filtered, and rotary evaporated to yield the crude diester as an oil. The crude diester was purified by column chromatography, with a petroleum spirit (40/60):diethyl ether eluent in a 80:20 ratio (for some diesters, a pet:ether 90:10 eluent gave better separation). Fragments were checked by TLC, recombined, and rotary evaporated to yield the pure diester dioneopentyl maleate as a white solid (7.250 g 90% yield, Found: C, 63.15; H, 5.4. Calc. for  $C_{14}H_{24}O_4$ : C, 63.2; H, 5.3%). Yields, elemental analysis and full  $^1H$  NMR analysis for all diesters can be found in the supporting information.

Bis(2,2-dimethylpropanol) fumarate (7.250 g, 1.0 eq.) was then dissolved in a 1:1 mixture of ethanol/water (250 mL) and refluxed. Sodium metabisulfite (9.229 g, 1.1 eq.) and sodium sulphite (4.464 g, 0.9 eq.) were added portion-wise during the first hour of reflux. The reaction was monitored by TLC (eluting with ethyl acetate). If some residual diester remained after 2 hours, additional disulfite and sulphite were added. Once complete, the reaction mixture was decanted off and rotary evaporated.

### 2.2.1 Surfactant purification.

To remove residual inorganic material left over from the sulfonation step, soxhlet extraction with ethyl acetate was performed for 24 hours. Then, once rotary evaporated, the product from soxhlet extraction was dissolved in the minimum amount of methanol and centrifuged at 6000 rpm for 45 minutes. The reaction mixture was decanted leaving any residual salt, rotary evaporated, and dried in the oven overnight (60 °C, 15 mbar). The product from centrifugation was recrystallised from either methanol or ethanol, and then dried under vacuum for at least 24 hours (60 °C, 15 mbar) to yield the pure surfactant AOTA as a white solid (6.103 g 84% yield). Found: C, 46.86; H, 7.09; S, 8.64. Calc. for  $C_{14}H_{25}NaO_7S$ : C, 46.66; H, 6.99; S, 8.90%.  $^1H$  NMR (400 MHz, DMSO- $d_6$ )  $\delta$  0.84-0.88 [d, 18H],  $\delta$  2.71-2.89 [dd, 2H],  $\delta$  3.58-3.62 [dd, 1H],  $\delta$  3.92-4.05 [m, 4H]. Once dried, the final products were stored in sealed vials in a desiccating cabinet over refreshed phosphorus pentoxide. Yields, elemental analysis and full  $^1H$  NMR analysis for all diesters can be found in the supporting information. All purified surfactants were investigated with a range of analytical methods,  $^1H$ ,  $^{13}C$  and EA (elemental analysis), which confirmed the desired products at 98% purity. All experimental data can be found within † (Electronic supplementary information - ESI).

### 2.3 Surface tension

Surface measurements were made using a K100 tensiometer at the Krüss Surface Science centre at the University of Bristol, using the Wilhelmy plate method. Glassware was repeatedly cleaned with a dilute Decon solution - methanol - ultra pure water cycle (Millipore, 18.2 M $\Omega$ cm) until a surface tension of 72.0  $\pm$  0.2 mNm $^{-1}$  at 25 °C was obtained. Prior to the surface tension isotherm being determined, the appropriate amount of EDTA (ethylenediaminetetraacetic acid tetrasodium salt hydrate) must be determined individually for each surfactant, on a batch-by-batch basis. The appropriate molar ratio of surfactant:EDTA must be determined to sequester any polyvalent cations which may be

present at the surface, but without exerting any electrolyte effect. The procedure is described in more detail here (ref. 16). Surface tension measurements were then carried out at the following surfactant:EDTA ratio - AOTA (275:1), AOTSiA (300:1), AOTB (425:1), AOTSiB (500:1) and AOTSiC (250:1). Repeat measurements were made at each concentration until the surface tension was constant. All measurements were made at 25 °C  $\pm$  0.2 °C using a Grant LTD6G circulating water bath.

### 2.4 Small-Angle Neutron Scattering (SANS)

SANS measurements were performed on D33 at the Institute Laue-Langevin (ILL, Grenoble, France) and SANS 2D at the ISIS facility (Rutherford Appleton Laboratory, Didcot, UK). The D33 instrument used neutrons with a wavelength of  $\lambda = 6$  Å and two sample-detector positions (2 and 7.5 m) providing an accessible Q range of 0.005-0.2 Å $^{-1}$ . On SANS 2D, a simultaneous Q-range of 0.004-0.6 Å $^{-1}$  was achieved with a neutron wavelength range of 1.75 <  $\lambda$  < 15.5 Å and a source-sample-detector distance L1=L2=4m. All samples were made in D $_2$ O, using 2 mm path length rectangular quartz cells at a temperature of 60 °C. Raw SANS data were reduced by subtracting the scattering of the empty cell and D $_2$ O background and normalised to an appropriate standard using the instrument-specific software. SANS data were fit using SasView. For all concentrations of AOTB, SiA and SiB, and intermediate concentrations of AOTA / SiC, the elliptical form factor model was applied. Data at high concentrations of AOTSiC were fit to a lamella paracrystal form factor which models repeating stacks of lamellar sheets. Finally, low concentrations of AOTSiC and AOTA were fit to a spherical form factor. Full details of models used can be found in † (ESI) as well as the following references: Lamellar paracrystal model - Bergstrom<sup>20</sup> and Kotlarchyk,<sup>21</sup> Ellipsoid model - Feigin,<sup>22</sup> Sphere model - Guiner.<sup>23</sup>

## 3 Results and discussion

### 3.1 Equilibrium surface tension

Determining surface properties from tensiometric experiments relies on the observation that increasing surfactant concentration causes a decrease in the surface tension until a break point is reached at the cmc. It is assumed the interface and bulk phases are in equilibrium, the surface coverage can be determined indirectly using the Gibbs adsorption equation, which relates the surface excess  $\Gamma$  (molm $^{-2}$ ) to changes in the surface tension  $\gamma$  (Nm $^{-1}$ ):

$$\Gamma = -\frac{1}{mRT} \frac{d\gamma}{d(\ln a)} \quad (1)$$

where  $a$  = solute activity and  $m$  = the theoretical prefactor. For ionic surfactants, the importance of using activity in the Gibbs equation over concentration has already been established.<sup>24</sup> Therefore, the Debye-Hückel limiting law was used to calculate solute activity. The theoretical prefactor,  $m$ , is dependent on the surfactant type and structure.<sup>25</sup> For a 1:1 ionic surfactant in the absence of any extra electrolyte, this prefactor is 2. The average area occupied per surfactant molecule at the cmc,  $A_{cmc}$ , can then be found:

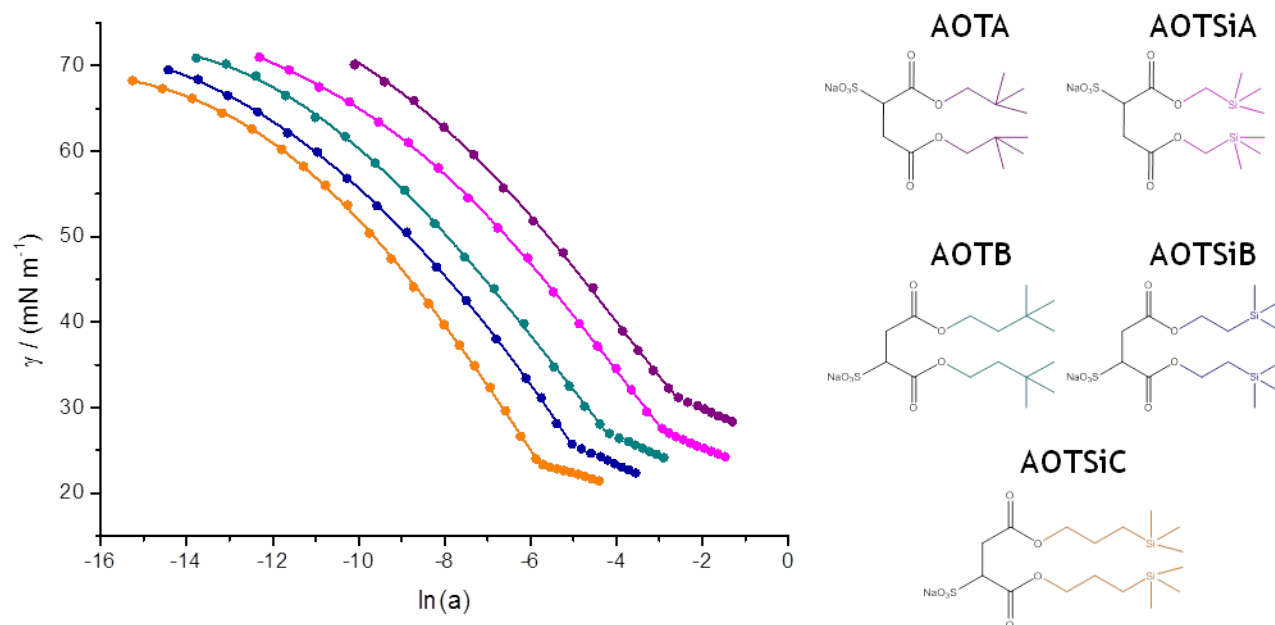


**Fig. 2** Equilibrium surface tension data from right to left for AOTA, AOTSiA, AOTB, AOTSiB and AOTSiC at 25 °C in water at EDTA:surfactant ratios as noted in the Experimental section. Polynomial lines fit to pre-cmc data are shown. Surfactant molecular structures are also included, the colour of the tail corresponds to the appropriate curve. Curves slightly off-set to improve clarity between surfactants with similar cmcs.

$$A_{\text{cmc}} = \frac{1}{\Gamma_{\text{cmc}} N_{\text{A}}} \quad (2)$$

where  $\Gamma_{\text{cmc}}$  is the surface excess at the cmc and  $N_{\text{A}}$  is Avogadro's constant. As discussed previously in section 2.3, to ensure a chemically pure surface free from polyvalent  $M^{n+}$  species that are inevitably introduced during synthesis, the appropriate surfactant:EDTA ratios must be determined separately for each surfactant on a batch-by-batch basis. Equilibrium  $\gamma$  vs  $\ln a$  plots for the TMS-hedgehogs are shown in Figure 2. All curves show clean breaks at the cmc with no minima or shoulders which would indicate surface-active impurities. CMCs were determined by taking the double differential of the surface tension data with respect to activity, and then applying a Gaussian distribution function, where the minima was taken to be the value of cmc, example shown in †(ESI). The pre-cmc data were fit to quartic functions to estimate the limiting surface excess concentration at the cmc, and thus, the area per molecule at the cmc. These results are given in Table 1.

For linear surfactants, the cmc decreases logarithmically with increasing linear alkyl chain length, consistent with the Kleven equation.<sup>26</sup> For branched surfactants, the link between cmc and alkyl carbon number is typically not so simple. Comparison of the cmc data presented in Table 1 shows a logarithmic decrease with increasing chain length (e.g. AOTA/AOTB), due to an increase in hydrophobicity. For AOTSiA, SiB and SiC each tail possesses effectively 5, 6 and 7 carbons, with cmcs proportional to their linear analogues (ref 9). As expected, incorporating silicon into the chains (AOTA/AOTSiA) causes further decreases in cmc.

The performance of linear vs branched surfactants can be compared through their effectiveness, i.e.  $\gamma_{\text{cmc}} - \gamma$  at the common reference concentration cmc. For linear surfactants, the general

**Table 1** Surface properties determined from  $\gamma$  vs  $\ln a$  plots for each surfactant at 25 °C. Data for AOT<sup>9</sup>, SDS<sup>27</sup>, and SS1<sup>28</sup>.

Surfactant	cmc (mM) ± 0.2	$\gamma_{\text{cmc}}$ (mN m <sup>-1</sup> ) ± 0.1	$A_{\text{cmc}}$ (Å <sup>2</sup> ) ± 2
AOTA	89.6	30.2	79
AOTSiA	68.1	27.0	82
AOTB	25.9	26.7	75
AOTSiB	15.9	24.3	78
AOTSiC	3.0	22.8	74
AOT	2.56	30.8	75
SDS	8.15	31.2	47
SS1	-	21.5	70

trend is a slight decrease in  $\gamma_{\text{cmc}}$  with increasing carbon number, reflecting an increase in the chain density present in the surface films.<sup>29</sup> For branched surfactants, both the specific positions and extent of chain branching play important roles, due to the imposed geometrical constraints which affect how surfactant molecules pack (ref 9). Branching near the chain tips produces increases in effectiveness, highlighted by the fact that all current super-efficient hydrocarbon surfactants possess fully branched chain tips, i.e. the maximum number of three  $-\text{CH}_3$  groups in the chain tips (refs. 10, 11). This improvement in effectiveness is thought to be due to a direct increase in the  $-\text{CH}_3$  to  $-\text{CH}_2-$  ratio per headgroup based on the following order of increasing surface energy  $\text{CF}_3 < \text{CF}_2 < \text{CH}_3 < \text{CH}_2$  (ref 13). The *t*-butyl group has the highest  $\text{CH}_3$  content of any alkyl moiety, and is therefore suitably equipped to produce dense surface layers populated by low surface energy  $\text{CH}_3$  groups.

All of the surfactants reported here possess either a *t*-butyl or

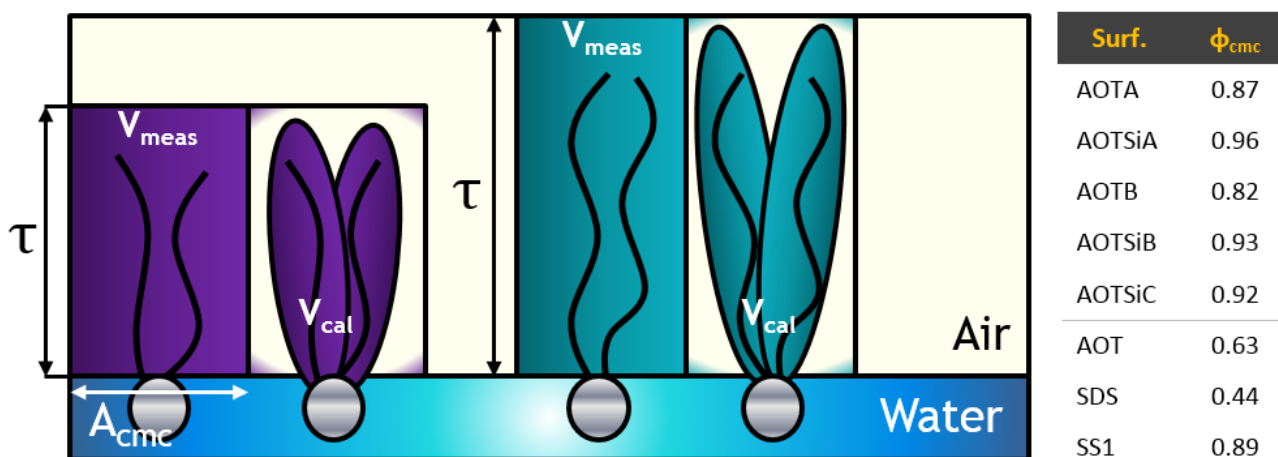


**Fig. 3** Visual representation of surfactants at the air-water interface, showing the different fragments and interfacial volumes used in the calculation of  $\Phi_{\text{cmc}}$ . The measured surfactant volume is  $V_{\text{meas}}$  and the calculated volume based on the summation of fragments is  $V_{\text{cal}}$ . Calculated surface coverages for the hybrid series at 25 °C are also shown, as well as AOT<sup>9</sup>, SDS<sup>27</sup> and SS1<sup>28</sup>.

trimethylsilyl group at the chain tip. From the  $\gamma_{\text{cmc}}$  values shown in Table 1, AOTSiC is the strongest performer achieving  $\gamma_{\text{cmc}} = 22.8 \text{ mN m}^{-1}$ , the lowest currently reported for a hydrocarbon surfactant (ref. 14). There is a clear decrease in  $\gamma_{\text{cmc}}$  as chain length increases, which is counterintuitive as the  $-\text{CH}_3:-\text{CH}_2-$  decreases suggesting sufficiently long tails are required to achieve low  $\gamma_{\text{cmc}}$ . Longer tails could screen underlying polar interactions more effectively, or possess a greater conformational freedom, which could allow a greater packing efficiency. However, long chains in the surfactant tails are not a prerequisite of low surface energy. The short chain hedgehog surfactant di-BC<sub>6</sub>SS shares a very similar tail structure to AOTA (possessing simply one extra CH<sub>3</sub> group) but achieves  $\gamma_{\text{cmc}} = 23.8 \text{ mN m}^{-1}$  (at 35 °C - ref. 11). On comparison with AOTA, reaching  $\gamma_{\text{cmc}} = 30.2 \text{ mN m}^{-1}$ , the difference of 6  $\text{mN m}^{-1}$  for such a simple difference in molecular structure is remarkable. Possibly because the tail structure of di-BC<sub>6</sub>SS is close to a maximum  $-\text{CH}_3:-\text{CH}_2-$  ratio; future work aims to elucidate this. When compared to the surface properties of a common linear or branched HC surfactant, such as SDS or AOT respectively, or a common reference silicone surfactant SS1 (data shown in Table 1), the TMS-hedgehog series produce a more effective reduction of  $\gamma$ . Generating surface tensions far below the commonly achieved value of  $\approx 30 \text{ mN m}^{-1}$  for HC surfactants.

It is thought that one reason FC surfactants display the most efficient reduction of surface tension is due to the larger atomic volume of fluorine over hydrogen ( $-\text{CH}_2- = 27 \text{ \AA}^3 / -\text{CF}_2- = 38 \text{ \AA}^3$ ).<sup>30</sup> Compared to a HC analogue, a fluorocarbon chain will have a larger cross sectional area, a lower packing density per unit area and therefore, less intermolecular interactions per unit area. As highlighted, the *t*-butyl and trimethylsilyl groups are effective alkyl moieties to help generate dense surface layers populated by low surface energy CH<sub>3</sub> groups. Silicon has a larger atomic radius than carbon and hence, replacing carbon in the *t*-butyl group with silicon should generate a more efficient reduction of  $\gamma_{\text{cmc}}$ . From Table 1, there is a clear decrease in  $\gamma_{\text{cmc}}$  when silicon is incor-

porated into the surfactant tail. This suggests a lower packing density per unit area when silicon is present in the chain tip. Furthermore, the area per molecule decreases with increasing chain length, suggesting more tightly packed molecules, given the increase in molecular volume. Similar trends have been found for other surfactant systems due to a decrease in chain rigidity, and a change in the hydration structure of the headgroups.<sup>31</sup>

### 3.2 Surface coverage

One of the clearest ways of characterising an adsorbed layer is in terms of the limiting  $A_{\text{cmc}}$ , determined from the surface excess at the cmc  $\Gamma_{\text{cmc}}$ , as this gives an indication about how the molecular structure affects packing at the interface. From Table 1, comparing  $A_{\text{cmc}}$  for a TMS and purely HC hedgehog shows a change on the order of the experimental uncertainty, e.g. AOTA  $A_{\text{cmc}} = 79$  and AOTSiA  $A_{\text{cmc}} = 82 \text{ \AA}^2$ . From the area per molecule, the surface coverage at the cmc  $\Phi_{\text{cmc}}$  can be determined, defined as:

$$\Phi_{\text{cmc}} = \frac{V_{\text{cal}}}{V_{\text{meas}}} \quad (3)$$

where  $V_{\text{cal}}$  is the total physical volume of surfactant molecular fragments,<sup>32-34</sup> and  $V_{\text{meas}}$  is the total volume occupied by a molecule at the air-water interface, calculated from:

$$V_{\text{meas}} = A_{\text{cmc}} \times \tau \quad (4)$$

$A_{\text{cmc}}$  has been defined and  $\tau$  is an interfacial thickness which can be estimated using the Tanford equation (ref. 34) or determined by neutron reflectivity (e.g. ref. 32). An illustration of these volumes and dimensions is presented in Figure 3, as well as corresponding  $\Phi_{\text{cmc}}$  data for the hedgehog series.

Values obtained for  $\Phi_{\text{cmc}}$  are then an intrinsic property and independent of both surfactant geometry and chemistry of the surfactants. Assuming the layer is uniform, a high  $\Phi_{\text{cmc}}$  ( $\rightarrow 1$ ) indicates an efficiently packed monolayer with little free space. Previous work which highlighted the first general structure-property relationship of surface tension suggests that a low surface tension

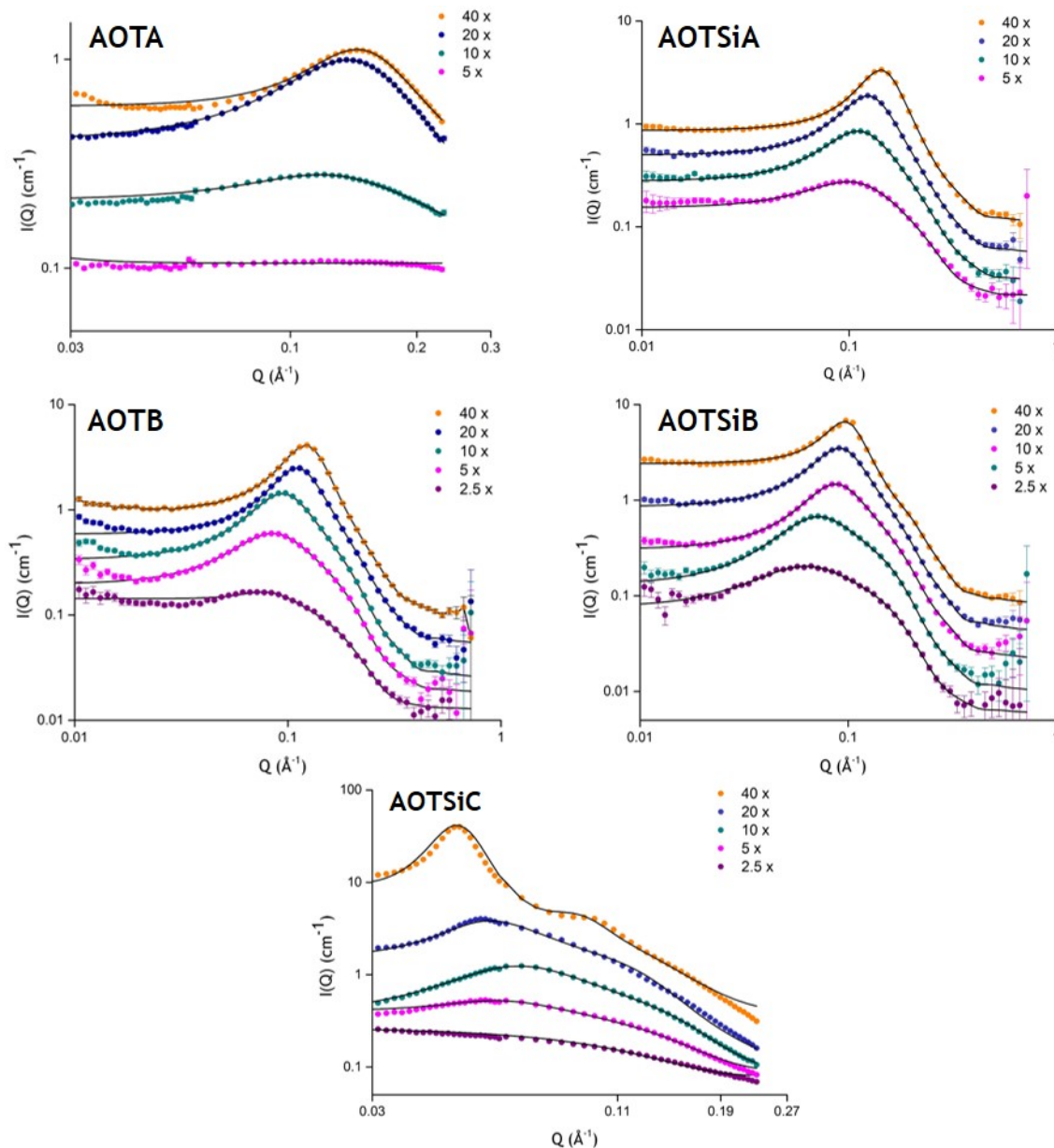


**Fig. 4** SANS profiles for AOTA, AOTSiA, AOTB, AOTSiB and AOTSiC in  $D_2O$  over a range of concentrations which are consistent multiples of the cmc. Measurements were made at  $60^\circ C$  to ensure a mono-phasic system for all concentrations. Data for AOTSiA, B and SiB are from SANS 2D, ISIS. Data for AOTA and AOTSiC are from D33, ILL.

is achieved by efficient monolayer packing, regardless of surfactant type (ref. 14). From the data presented in Figure 3, the TMS-hedgehog series all pack efficiently at the surface, producing high  $\Phi_{cmc}$  values which are comparable with the super-efficient FC surfactant di-CF4 ( $\gamma_{cmc} = 17.7 \text{ mNm}^{-1}$   $\Phi_{cmc} = 0.97$ )<sup>35</sup>. Furthermore, if the TMS-hedgehog is compared to the purely HC analogue, for example AOTA versus AOTSiA, from the  $A_{cmc}$  data shown in Table 1, one might expect AOTSiA to produce a lower  $\Phi_{cmc}$  given the larger  $A_{cmc}$  and hence  $V_{meas}$ . However, it is clear that the presence of silicon in the chain in place of carbon improves packing efficiency and surface coverage (i.e.  $\Phi_{cmc} \rightarrow 1$ ). Thus, the lower  $\gamma_{cmc}$  and higher  $\Phi_{cmc}$  generated by AOTSiA over AOTA, can be attributed to the larger size of silicon ( $r_{Si} = 1.1 \text{ \AA}$ )

compared to carbon ( $r_{Si} = 0.7 \text{ \AA}$ ) which helps fill the space between surfactant tails, due to the increased molecular volume of the chain tips. The least efficient surfactant of this series, AOTA, produces one of the lowest values of  $\Phi_{cmc}$ . Compared to the very similar analogue di-BC<sub>6</sub>SS, which achieves  $\gamma_{cmc} = 23.8 \text{ mNm}^{-1}$ , a more efficiently packed monolayer is formed -  $\Phi_{cmc} = 0.95$  (ref. 14). This suggests that for small branched hydrocarbon surfactants, a low surface energy can be achieved by either a) a highly branched tail with a  $CH_3$  to  $CH_2$  ratio close to 1 (i.e. di-BC<sub>6</sub>SS), or b) a sufficiently long and thus flexible tail with a high  $CH_3$  to  $CH_2$  ratio in the chain tip (i.e. AOTSiC). When comparing  $\Phi_{cmc}$  values with the common surfactants AOT, SDS, and SS1, the relationship between high surface coverage and low surface tension

**Table 2** SANS Parameters fit to the Charged Ellipsoid or Sphere models and Lamella stacks model for the hedgehog series in D<sub>2</sub>O at 60 °C

Parameter	AOTSiA					AOTB					AOTSiB				
	40x	20x	10x	5x	2.5x	40x	20x	10x	5x	2.5x	40x	20x	10x	5x	2.5x
R <sub>eq</sub> (Å) ± 0.1	16.9	16.7	16.2	14.6	-	19.1	18.9	18.5	17.5	16.3	24.3	22.1	20.3	19.3	18.0
R <sub>pol</sub> (Å) ± 0.1	8.2	8.0	7.5	7.1	-	9.1	8.9	8.9	8.7	8.3	9.5	9.8	9.2	9.3	8.9
X	2.06	2.09	2.16	2.06	-	2.10	2.12	2.08	2.01	1.96	2.56	2.26	2.21	2.08	2.02
Z ± 0.5	15	13	11	10	-	32	21	18	11	9	36	24	18	13	12
	AOTA				AOTSiC										
	40x	20x	10x	5x	40x	20x	10x	5x	2.5x						
R <sub>eq</sub> (Å) ± 0.1	14.4	13.8	9.3	-	-	25.5	22.3	21.1	-						
R <sub>pol</sub> (Å) ± 0.1	9.8	8.3	8.2	-	-	11.2	9.3	11.0	-						
X	1.50	1.66	1.13	-	-	2.28	2.40	1.92	-						
Z ± 0.5	14	10	8	-	-	17	14	16	-						
R <sub>sphere</sub> (Å) ± 0.1	-	-	-	9.4	-	-	-	-	19.1						
D (Å) ± 0.002	-	-	-	-	22.1	-	-	-	-						
L (Å) ± 0.004	-	-	-	-	129.3	-	-	-	-						
N <sub>layer</sub> (Å) ± 0.01	-	-	-	-	11.1	-	-	-	-						
P	-	-	-	-	0.19	-	-	-	-						

is clearly highlighted, i.e. AOT -  $\gamma_{\text{cmc}} = 30.8 \text{ mN m}^{-1}$   $\Phi_{\text{cmc}} = 0.63$  and AOTSiB  $\gamma_{\text{cmc}} = 24.3 \text{ mN m}^{-1}$   $\Phi_{\text{cmc}} = 0.93$ .

By comparing the surface tension data, there is no evidence to suggest silicon induces strong dipoles in the chain tips, due to the lower surface energies achieved by the trimethylsilyl analogues. Therefore, the low surface energies achieved by these TMS-hedgehogs can be attributed to an increased molecular volume which improves packing efficiency between surfactant tails in the surface monolayers leading to a higher surface coverage.

### 3.3 Small-Angle Neutron Scattering

It is of interest to see if the subtle changes in molecular structure affect surfactant aggregation and preferred micellar shape, hence, Small-angle neutron scattering (SANS) data were collected as a function of concentration. Measurements were made at 60 °C for all surfactants to ensure complete solubility in D<sub>2</sub>O. Concentrations were kept consistent at multiples above the cmc (i.e. 40x, 20x etc). Scattering profiles with corresponding fits are shown in Figure 4. For AOTA/AOTSiA, the most dilute concentration did not scatter strongly enough and these data are not included.

The scattering profiles for AOTB, AOTSiA and AOTSiB are well described as oblate ellipsoid form factors with charged structure factors to account for repulsion. The parameters used to model the charged oblate ellipsoids - equatorial radius [R<sub>eq</sub> / Å], polar radius [R<sub>pol</sub> / Å], aspect ratio [X = R<sub>eq</sub> / R<sub>pol</sub>] and effective micellar charge (Z). For AOTA and AOTSiC the shape of the aggregates change with varying concentration. Oblate charged ellipsoids are still formed, but at low concentrations, a more spherical shape is observed and interestingly, for AOTSiC at the highest concentration, a lamella structure is formed. To model the lower concentrations of AOTA and AOTSiC a spherical model was used for the radius - [R<sub>sphere</sub> / Å], and to model the lamellar structures present at the highest concentration of AOTSiC, a paracrystal lamellar model was used (ref. 20) with the following

parameters - bilayer thickness [D - Å], average distance between two adjacent layers [L - Å], distribution of layer distance [P], and number of layers [N<sub>layers</sub>]. These data are shown in Table 2.

From Figure 4 all surfactants show an intermediate-Q peak which is characteristic of charged micelles. As the concentration increases this intermediate peak becomes more pronounced and moves to higher Q. For each surfactant, the sizes of the ellipsoids determined from the fits follows the expected trend, with the smallest surfactants forming the smallest micelles (e.g. AOTA ≈ 10 Å). The charge is also seen to decrease in accordance with decreasing micelle size. AOTSiA, AOTB and AOTSiB only form oblate ellipsoids which display common behaviour for charged anisotropic micelles when concentration is varied. Similar trends have been reported before for other surfactant systems including the common linear HC surfactant SDS.<sup>36-39</sup> For AOTA and AOTSiC, charged oblate ellipsoids are formed in the intermediate concentration regime which follow the expected trend.

The sizes and shapes of micelles depends on a balance of interactions between molecular structure of the surfactant tail, and repulsion between headgroups. At low concentrations of AOTA, the intermediate-Q peak is lost, due to weaker repulsion between neighbouring micelles. From the aspect ratio values in Table 2, there is a shape transition from ellipsoidal to spherical as concentration decreases. The same is true for AOTSiC in the low concentration regime, forming spherical micelles with radii ≈ 19.1 Å. This transition in shape is possibly due to the weaker charge on the micelles, reducing repulsion between neighbouring headgroups.

For AOTSiC the intermediate-Q peak moves to lower Q as concentration is increased, showing the presence of larger aggregates. At the highest concentration (40 x cmc) a clear Bragg peak can be seen which is characteristic of d-spacing between lamellae. The average number of layers is around 11, indicating a large structure formed from many stacks of lamellar sheets with an average bilayer thickness of 22.1 Å. The average distance between



layers obtained by the model agrees well with the estimated distance from the Q-value of the highest peak. Previous SANS studies of large, bulky hedgehog surfactants reported the formation of lamellar structures (ref. 10). The transition to lamellar structures at high concentration has been reported before,<sup>40</sup> and is due to significant interactions between micelles that become overpacked above a certain concentration.

Overall the subtle differences in molecular architecture of the surfactants discussed here do not seem to greatly affect the shapes of the micellar aggregates formed. The effect of concentration and micellar charge play bigger roles. Incorporating silicon into the chain tip only causes a slight increase in the micelle size. Highlighting that when nearing the limit of performance achievable with hydrocarbon surfactants, the relationship between molecular structure and packing is extremely sensitive in the surface monolayer, compared to micellar packing in solution.

## 4 Conclusion

The general structure-property relationship for surface tension indicates that low surface energies are achieved through efficient packing between surfactant molecules in the orientated surface monolayers (ref. 14). Here, this relationship has been extended and reinforced through a novel approach to improving packing efficiency, namely, replacing a carbon atom in the chain tips with silicon. This leads to increased molecular volumes of the surfactant tails, increased surface coverage, and consequently, a lower surface tension (AOTSiC  $\gamma_{\text{cmc}} = 22.8 \text{ mNm}^{-1}$ ).

The super efficient hydrocarbon surfactant, di-BC<sub>6</sub>SS, highlighted that short branched tail structures can effectively reduce aqueous surface tension (ref. 11). By comparing the structure-performance of the most effective hydrocarbon surfactants, the trimethylsilyl and *t*-butyl groups are shown to be effective and necessary alkyl moieties to help achieve low surface energies with HC surfactants. This has been highlighted in terms of limiting surface coverage,  $\Phi_{\text{cmc}}$ , where the TMS-hedgehogs all show efficient packing in the monolayers (i.e. high  $\Phi_{\text{cmc}}$ ). **Furthermore, the effective performance of this new HC surfactant series is highlighted by comparing with standard surfactants such as AOT or SDS, i.e. AOT -  $\gamma_{\text{cmc}} = 30.8 \text{ mNm}^{-1}$   $\Phi_{\text{cmc}} = 0.63$  and AOTSiB  $\gamma_{\text{cmc}} = 24.3 \text{ mNm}^{-1}$   $\Phi_{\text{cmc}} = 0.93$ .**

Through the use of Small-angle neutron scattering (SANS), these hydrocarbon surfactants have been shown to generally form oblate ellipsoidal micelles. However, for some, as the concentration is varied, different aggregation structures form including lamellae and spherical micelles (ref. 37 & 41).

Previous studies have examined the effects of chain branching on surface tension (ref. 10 & 9). This study highlights the sensitivity of the relationship between surface energy and structure when designing surfactants close to the limit of their performance. These results point to new ways of effectively controlling surface energy through the design of environmentally acceptable, commercially viable, super-effective 21st century surfactants.

## References

- 1 M. J. Rosen and Z. H. Zhu, *J Am Oil Chem Soc*, 1988, **65**, 663–668.
- 2 T. Zhang and R. E. Marchant, *Journal of colloid and interface science*, 1996, **177**, 419–426.
- 3 R. M. Manglik, V. M. Wasekar and J. Zhang, *Experimental thermal and fluid science*, 2001, **25**, 55–64.
- 4 G. Para, E. Jarek and P. Warszynski, *Colloids and Surfaces A: Physicochemical and Engineering Aspects*, 2005, **261**, 65–73.
- 5 P. Brown, C. Butts, R. Dyer, J. Eastoe, I. Grillo, F. Guittard, S. Rogers and R. Heenan, *Langmuir*, 2011, **27**, 4563–4571.
- 6 L. L. Schramm, E. N. Stasiuk and D. G. Marangoni, *Annual Reports Section "C"(Physical Chemistry)*, 2003, **99**, 3–48.
- 7
- 8 J. M. Conder, R. A. Hoke, W. d. Wolf, M. H. Russell and R. C. Buck, *Environmental science & technology*, 2008, **42**, 995–1003.
- 9 S. Nave, J. Eastoe and J. Penfold, *Langmuir*, 2000, **16**, 8733–8740.
- 10 S. Alexander, G. N. Smith, C. James, S. E. Rogers, F. Guittard, M. Sagisaka and J. Eastoe, *Langmuir*, 2014, **30**, 3413–3421.
- 11 M. Sagisaka, T. Narumi, M. Niwase, S. Narita, A. Ohata, C. James, A. Yoshizawa, E. Taffin de Givenchy, F. Guittard, S. Alexander *et al.*, *Langmuir*, 2014, **30**, 6057–6063.
- 12 F. M. Fowkes, *The Journal of Physical Chemistry*, 1963, **67**, 2538–2541.
- 13 W. A. Zisman, *Contact angle, Wettability and Adhesion*.
- 14 A. Czajka, G. Hazell and J. Eastoe, *Langmuir*, 2015, **31**, 8205–8217.
- 15 T. Goloub, R. Pugh and B. Zhmud, *Journal of colloid and interface science*, 2000, **229**, 72–81.
- 16 J. Eastoe, S. Nave, A. Downer, A. Paul, A. Rankin, K. Tribe and J. Penfold, *Langmuir*, 2000, **16**, 4511–4518.
- 17 S. Gold, J. Eastoe, R. Grilli and D. C. Steytler, *Colloid and polymer science*, 2006, **284**, 1333–1337.
- 18 M. Knoche, H. Tamura and M. J. Bukovac, *Journal of agricultural and food chemistry*, 1991, **39**, 202–206.
- 19 N. Yoshino, N. Komine, J.-i. Suzuki, Y. Arima and H. Hirai, *Bulletin of the chemical society of Japan*, 1991, **64**, 3262–3266.
- 20 M. Bergström, J. S. Pedersen, P. Schurtenberger and S. U. Egelhaaf, *The Journal of Physical Chemistry B*, 1999, **103**, 9888–9897.
- 21 M. Kotlarchyk and S. Ritzau, *Journal of Applied Crystallography*, 1991, **24**, 753–758.
- 22 L. Feigin, D. I. Svergun and G. W. Taylor, *Structure analysis by small-angle X-ray and neutron scattering*, Springer, 1987.
- 23 A. Guiner, G. Fournet and C. Walker, *J. Wiley & Sons, New York*, 1955.
- 24 R. Strey, Y. Viisanen, M. Aratono, J. P. Kratochvil, Q. Yin and S. E. Friberg, *The Journal of Physical Chemistry B*, 1999, **103**, 9112–9116.
- 25 S. An, J. Lu, R. Thomas and J. Penfold, *Langmuir*, 1996, **12**, 2446–2453.
- 26 H. Klevens, *Journal of the American Oil Chemists Society*, 1953, **30**, 74–80.
- 27 J. R. Lu, A. Marrocco, T. J. Su, R. K. Thomas and J. Penfold, *Journal of colloid and interface science*, 1993, **158**, 303–316.

- 28 K. Ananthapadmanabhan, E. Goddard and P. Chandar, *Colloids and Surfaces*, 1990, **44**, 281–297.
- 29 A. Pitt, S. Morley, N. Burbidge and E. Quickenden, *Colloids and Surfaces A: Physicochemical and Engineering Aspects*, 1996, **114**, 321–335.
- 30 M. P. Krafft and J. G. Riess, *Chemical reviews*, 2009, **109**, 1714–1792.
- 31 K. Lunkenheimer, K. Haage and R. Hirte, *Langmuir*, 1999, **15**, 1052–1058.
- 32 Z. Li, J. Lu, R. Thomas and J. Penfold, *The Journal of Physical Chemistry B*, 1997, **101**, 1615–1620.
- 33 S. S. Berr and R. R. Jones, *The Journal of Physical Chemistry*, 1989, **93**, 2555–2558.
- 34 C. Tanford, *The Journal of Physical Chemistry*, 1972, **76**, 3020–3024.
- 35 J. Eastoe, A. Downer, A. Paul, D. C. Steytler, E. Rumsey, J. Penfold and R. K. Heenan, *Physical Chemistry Chemical Physics*, 2000, **2**, 5235–5242.
- 36 E. G. R. Putra and A. Ikram, *Indonesian Journal of Chemistry*, 2010, **6**, 117–120.
- 37 B. Hammouda, *Journal of research of the National Institute of Standards and Technology*, 2013, **118**, 151.
- 38 L. L. Brasher and E. W. Kaler, *Langmuir*, 1996, **12**, 6270–6276.
- 39 V. Aswal and P. Goyal, *Chemical physics letters*, 2003, **368**, 59–65.
- 40 P. Kekicheff, C. Grabielle-Madelmont and M. Ollivon, *Journal of Colloid and Interface Science*, 1989, **131**, 112–132.
- 41 B. Hammouda, *The Journal of chemical physics*, 2010, **133**, 084901.